

Low lattice thermal conductivity and high figure of merit in p-type doped K_3IO

Weiqiang Wang(王巍强), Zhenhong Dai(戴振宏), Qi Zhong(钟琦), Yinchang Zhao(赵银昌), and Sheng Meng(孟胜)

Citation: Chin. Phys. B, 2020, 29 (**12**): 126501. DOI: 10.1088/1674-1056/abab
Journal homepage: http://cpb.iphy.ac.cn; http://iopscience.iop.org/cpb

What follows is a list of articles you may be interested in

Low lattice thermal conductivity and high figure of merit in p-type doped K_3IO

Weiqiang Wang(王巍强), Zhenhong Dai(戴振宏), Qi Zhong(钟琦), Yinchang Zhao(赵银昌), and Sheng Meng(孟胜)
Chin. Phys. B, 2020, 29 (**12**): 126501. DOI: 10.1088/1674-1056/abab

Co-adsorption of O_2 and H_2O on α-uranium (110) surface: A density functional theory study

Xin Qu(瞿鑫), Ru-Song Li(李如松), Bin He(何彬), Fei Wang(王飞), Kai-Long Yuan(袁凯龙)
Chin. Phys. B, 2018, 27 (**7**): 076501. DOI: 10.1088/1674-1056/27/7/076501

Thermal transport in phosphorene and phosphorene-based materials: A review on numerical studies

Yang Hong(洪扬), Jingchao Zhang(张景超), Xiao Cheng Zeng(曾晓成)
Chin. Phys. B, 2018, 27 (**3**): 036501. DOI: 10.1088/1674-1056/27/3/036501

First-principles calculations of structural and thermodynamic properties of β-PbO

Vahedeh Razzazi, Sholeh Alaei
Chin. Phys. B, 2017, 26 (**11**): 116501. DOI: 10.1088/1674-1056/26/11/116501

Effects of in-plane stiffness and charge transfer on thermal expansion of monolayer transition metal dichalcogenide

Wang Zhan-Yu, Zhou Yan-Li, Wang Xue-Qing, Wang Fei, Sun Qiang, Guo Zheng-Xiao, Jia Yu
Chin. Phys. B, 2015, 24 (**2**): 026501. DOI: 10.1088/1674-1056/24/2/026501

Low lattice thermal conductivity and high figure of merit in p-type doped K_3IO*

Weiqiang Wang(王巍强)[1], Zhenhong Dai(戴振宏)[1,†], Qi Zhong(钟琦)[1], Yinchang Zhao(赵银昌)[1], and Sheng Meng(孟胜)[2,3,‡]

[1] *Department of Physics, Yantai University, Yantai* 264005, *China*
[2] *Beijing National Laboratory for Condensed Matter Physics and Institute of Physics, Chinese Academy of Sciences, Beijing* 100190, *China*
[3] *Collaborative Innovation Center of Quantum Matter, Beijing* 100084, *China*

(Received 24 June 2020; revised manuscript received 27 July 2020; accepted manuscript online 1 August 2020)

Based on first-principles calculations, Boltzmann transport equation and semiclassical analysis, we conduct a detailed study on the lattice thermal conductivity κ_L, Seebeck coefficient S, electrical conductivity σ, power factor $S^2\sigma$ and dimensionless figure of merit, zT, for K_3IO. It is found that K_3IO exhibits relatively low lattice thermal conductivity of 0.93 $W{\cdot}m^{-1}{\cdot}K^{-1}$ at 300 K, which is lower than the value 1.26 $W{\cdot}m^{-1}{\cdot}K^{-1}$ of the classical TE material PbTe. This is due to the smaller phonon group velocity v_g and smaller relaxation time τ_λ. The low lattice thermal conductivity can lead to excellent thermoelectric properties. Thus maximum zT of 2.87 is obtained at 700 K, and the $zT = 0.41$ at 300 K indicate that K_3IO is a potential excellent room temperature TE material. Our research on K_3IO shows that it has excellent thermoelectric properties, and it is a promising candidate for applications in fields in terms of thermoelectricity.

Keywords: first-principles calculation, lattice thermal transport, thermal transport characteristics, thermoelectric properties

PACS: 65.40.–b, 66.70.–f, 63.20.–e, 72.20.–i **DOI:** 10.1088/1674-1056/abab83

1. Introduction

As the supply of fossil fuels decreases and world demand increases, providing a sustainable energy to the world will become a major social problem in the 21st century.[1] Thermoelectric (TE) materials have played an important role in global sustainable energy solutions and have been continuously studied in recent decades. TE materials can generate electricity from waste heat. It provides a clean method for recovering waste heat from high-temperature industrial or transportation applications, so it is particularly important to find good thermoelectric materials.[2–4,39,40]

The efficiency of thermoelectric energy converters is limited by the thermoelectric properties ($zT = S^2\sigma T/\kappa$) of the materials, where S is Seebeck coefficient, σ is the electrical conductivity, T is the absolute temperature, and κ is the thermal conductivity, which consists of the lattice thermal conductivity κ_L and the electronic contribution κ_E.[5] Therefore, studying the thermal transport characteristics of electrons and lattices can reveal the complete TE performance. In addition, $S^2\sigma$ is called power factor (PF) and it is also used to estimate TE characteristics. Therefore, enhancing power factor (PF) and dimensionless figure of merit, zT, require a reasonable optimization combination of S, σ, and κ.

The research on TE materials are developed rapidly in the 1950s, and the basic science of TE materials was gradually improved. During this period, the Bi_2Te_3 compound and its alloys were discovered and reported to have the highest zT around 1.0. In the next forty years, there has not been much development in the field of TE materials, so $zT \approx 1$ has been considered as the benchmark for advanced TE materials.[6] The turning point occurred in the early 1990s when Hicks and Dresselhaus[7] pointed out that quantum mechanics can provide a new way for design of TE materials by reducing the number of dimensions. Later, it was proposed by different groups that low-dimensional materials have extremely high zT, which broke the limit of 1.0.[8,9,43] The idea of quantum effect promotes energy band engineering and nanostructure strategies, which can be applied to bulk thermoelectric materials.[10] After research and development in recent years, a large number of excellent TE materials have emerged, such as undoped monocrystalline SnSe at 923 K ($zT \sim 2.6$),[11] Na-doped PbTe at 773 K ($zT \sim 2.0$),[12] which have made great contribution to the development of sustainable energy in the world.

The antiperovskite structural material K_3IO has not been extensively studied, and its physical properties, especially thermoelectric properties, are extremely lacking. We predict by first-principles calculations that K_3IO has a relatively low lattice thermal conductivity and a large value of zT. The calculation method and details are described in Section 2. Results

*Project supported by the National Natural Science Foundation of China (Grant Nos. 11974302, 11774396, and 11704322) and the Shandong Natural Science Funds for Doctoral Program, China (Grant No. ZR2017BA017).

†Corresponding author. E-mail: zhdai@ytu.edu.cn
‡Corresponding author. E-mail: smeng@iphy.ac.cn

© 2020 Chinese Physical Society and IOP Publishing Ltd

and analyses of TE properties are presented in Section 3. The conclusion and summary are given in Section 4.

2. Methodology

We first study the thermal transport properties of K_3IO by solving the phonon Boltzmann transport equation (BTE)[14] and interatomic force constants (IFCs). The lattice thermal conductivity along the x direction can be defined as

$$\kappa_{\mathrm{L}}^{xx} = \frac{1}{k_{\mathrm{B}}T^2\Omega N}\sum_{\lambda} f_0(f_0+1)(\hbar\omega_\lambda)v_{\mathrm{g}}^{x,\lambda}F_\lambda^x, \tag{1}$$

where k_{B} is Boltzmann's constant, T is temperature, Ω is the volume of unit cell, N is the number of κ points of the first irreducible Brillouin zone; f_0 is the equilibrium Bose–Einstein distribution function, $\hbar$ is the reduced Planck constant, ω_λ is the phonon frequency of phonon mode λ, and $v_{\mathrm{g}}^{x,\lambda}$ is the phonon group velocity of phonon mode λ along the x direction. F_λ^α is defined as

$$F_\lambda^x = \tau_\lambda(v_{\mathrm{g}}^{x,\lambda} + \Delta_\lambda), \tag{2}$$

where τ_λ is the lifetime of phonon, and Δ_λ is a correction term.

We use the ShengBTE code to calculate the lattice thermal conductivity κ_{L}.[14] The harmonic (second-order) and anharmonic (third-order) interatomic force constants (IFCs) are calculated based on the density functional theory (DFT) through the combination of the Vienna *ab-initio* simulation package (VASP),[13] PHONOPY program,[15] and THIRDORDER.PY script.[14] The harmonic IFCs are calculated using $3\times3\times3$ supercells by finite-difference approach in the PHONOPY program. The anharmonic IFCs are obtained using $3\times3\times3$ supercells and Γ-point-only calculations via finite-difference approach in the thirdorder.py script, and the calculation of anharmonic IFCs includes interactions up to third nearest neighbors. The interaction between the ion cores and valance electrons is modeled by the projector augmented wave potentials[16] during the process of DFT calculations. The exchange-correlation functional of generalized gradient approximation (GGA) of Perdew–Burke–Ernzerhof (PBE)[18] and a plane-wave basis set with the cutoff energy of 520 eV are used to describe valence electrons. In order to optimize the primitive cell, the electronic convergence criterion is set to 10^{-8} eV and the force acting on each atom is less than 10^{-6} eV/Å. We utilize a $12\times12\times12$ Γ-centered Monkhorst–Pack k-point mesh grid to simulate the Brillouin zone integration of the primitive cell.

The electron Boltzmann theory and the rigid band approach in the BOLTZTRAP code[21] are used to calculate the electronic transport properties, k-point of $12\times12\times12$ is used to obtain the Kohn–Sham eigenvalues in the calculation of electronic structures. The scattering time τ determines the values of the conductivity σ and electronic thermal conductivity κ_{E}, which is the only empirical parameter in this approach. The scattering time τ can be estimated through the experimental values of carrier concentration n, mobility μ, and conductivity σ. Due to the lack of experimental data, the values of τ are 3 fs, 5 fs, 7 fs and 9 fs.

3. Results and discussion

As shown in Fig. 1, the antiperovskite structure K_3IO belongs to the cubic crystal system with the space group of $Pm\bar{3}m$ [221]. The primitive cell is composed of five atoms, the potassium, oxygen and iodine atom located at the center of the face, the center of the body and the apex of the primitive cell, respectively. In addition, the calculated lattice constant and band gap are 5.38 Å and 1.02 eV, respectively. Since the band gap calculated by the DFT method will be smaller than the GW method, we use the modified Becke–Johnson exchange potential (METAGGA = MBJ),[35,36] whose result is similar to that of the GW method, to recalculate the band gap and the result of the band gap is 1.32 eV (see Fig. S1 in the Supplementary Material). Although the band gap calculated by the DFT method is relatively small, it has almost no effect on the following calculations.

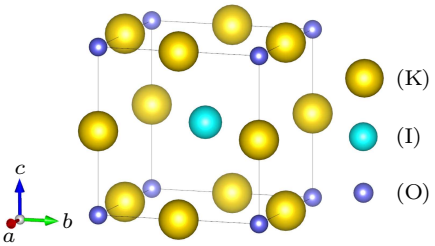


Fig. 1. The perspective view of crystal structure of antiperovskite structure K_3IO. The golden, blue and purple spheres represent K, I and O atoms, respectively.

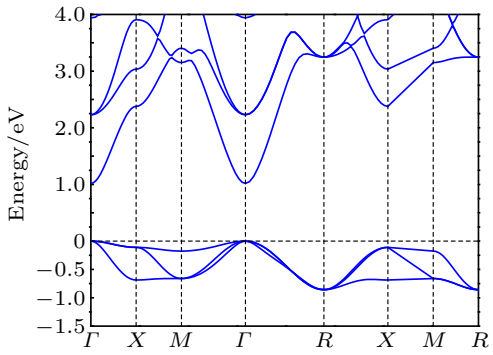


Fig. 2. Electronic energy band structure along a high-symmetry path in the first Brillouin zone of K_3IO.

Figure 2 shows electronic band structure of K_3IO. We can see from the electronic band structure that K_3IO belongs to direct band gap semiconductor, both the valence-band maximum (VBM) and conduction-band minimum (CBM) are located at the Γ point. The relatively flat band at the top of the valence band means a large effective mass, which usually

gives a large Seebeck coefficient of the material.[17] In addition, a notable feature is the relatively small effective mass caused by a highly dispersive pocket at the bottom of conduction band, which means high mobility and phonon group velocity. This allows the material to have excellent electrical conductivity. Therefore, the favorable condition for a better TE performance should be the combination of a high dispersion band at the bottom of the conduction band and a relatively flat band at the top of the valence band.[19,22]

The phonon dispersion relationship and partial phonon density of states (PDOS) of K_3IO are shown in Fig. 3. The phonon spectrum can be used to detect the stability of the structure. The stability of the crystal structure is that for each phonon mode, the frequency should be a real quantity, not an imaginary quantity.[23–26] For K_3IO, there is no imaginary frequency, so the dynamic stability of the material can be determined. Most of the acoustic modes are below 1.6 THz, showing a lower frequency, which usually means a lower Debye temperature. The Debye temperature Θ_D was calculated by the equation

$$\Theta_D = \frac{h\nu_m}{k_B}, \tag{3}$$

where h is the Planck constant, and ν_m is the highest frequency of atom elastic vibration. For K_3IO, the value of ν_m is 1.67 THz, the calculated Θ_D is 80.29 K. It can be seen from the PDOSs that the phonon state density is roughly divided into three regions as the frequency changes. The phonon frequencies of 0–2 THz is provided by the vibration of the I atom and the phonon frequencies of 2–6 THz and 6–9 THz are provided by the vibration of the K and O atoms, respectively. It means that almost all of the optic phonon modes are afforded by the light atoms (K and O atoms) and the acoustic phonon modes are afforded by the heavier atom (I atom).

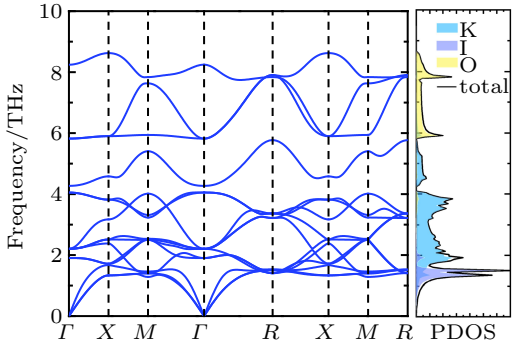


Fig. 3. Calculating phonon dispersion relations and partial phonon density of states (PDOS) of K_3IO along the high symmetry point within the first Brillouin zone.

Figure 4(a) gives the lattice thermal conductivity κ_L as a function of temperature T of K_3IO. We calculate the κ_L in the temperature range from 100 K to 700 K at intervals of 20 K. There is no obvious difference between the results of K_3IO's relaxation time approximation (RTA) and iterative solution (ITS). The iterative solution (ITS) is obtained by repeated calculations, where each calculated distribution function of Boltzmann transport equation is used as the initial value of the next iteration calculation until the final convergence result.[28] The κ_L (RTA) of K_3IO is 0.93 $W{\cdot}m^{-1}{\cdot}K^{-1}$ at 300 K, which is lower than the thermoelectric materials of PbTe (1.26 $W{\cdot}m^{-1}{\cdot}K^{-1}$),[27] PdTe (1.42 $W{\cdot}m^{-1}{\cdot}K^{-1}$ along x direction),[37] Na_2MgSn (1.77 $W{\cdot}m^{-1}{\cdot}K^{-1}$ along a axis),[33] PdSTe (5.45 $W{\cdot}m^{-1}{\cdot}K^{-1}$)[38] and NbP (2.0 $W{\cdot}m^{-1}{\cdot}K^{-1}$ along a axis).[42] The frequency-dependent normalized lattice thermal conductivity κ_L at 300 K is exhibited at Fig. 4(b), 85% of the lattice thermal conductivity is contributed by the phonon frequency of 0–3.85 THz. Combined with the phonon dispersions, we find that the lattice thermal conductivity κ_L is mainly dominated by potassium and oxygen atoms, while the high-frequency oxygen atoms are relatively less involved in the contribution of lattice thermal conductivity κ_L.

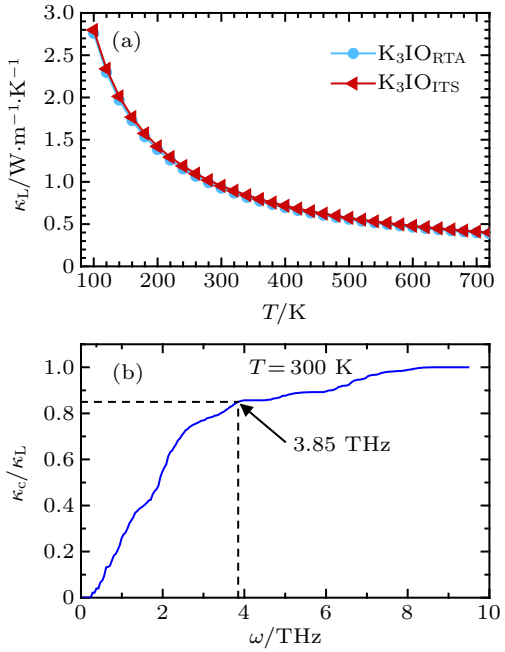


Fig. 4. (a) Lattice thermal conductivity κ_L for K_3IO. The blue circle and red triangle curves represent the RTA and ITS results of K_3IO, respectively. (b) The normalized lattice thermal conductivity κ_L as a function of phonon frequency at a temperature of 300 K.

To further understand the contribution of different phonon branches to the lattice thermal conductivity. Figure 5 shows the changes of phonon group velocity (a) and total relaxation time (b) with frequency for all phonon modes of K_3IO at 300 K. The phonon group velocity ν_g is an important factor that determines the thermal transport performance. From Figs. 3 and 4(b), we find three acoustic phonon modes dominate the heat transport in K_3IO. Therefore, we mainly discuss the transverse mode TA_1, the transverse mode TA_2 and the longitudinal mode LA, which is denoted by red triangles, yellow squares and green pentagons, respectively, other optic modes are indicated by blue five-pointed stars, as shown in Fig. 5(a), the

phonon group velocity is determined by phonon frequency. By comparison, we find that the phonon group velocities for phonon acoustic modes and optic modes of K_3IO are both less than that of PbTe.[27] In view of $\kappa_L \sim v_g^2$ in RTA, this is the primary factor that causes K_3IO to have a lower κ_L than PbTe.

To further detailed discuss the thermal transport mechanism, we show the total relaxation times of phonon modes as a function of frequency in Fig. 5(b). In the calculation of Sheng-BTE, due to the elimination of the boundary scattering effect, the total relaxation time in RTA can be obtained by

$$\frac{1}{\tau_\lambda} = \frac{1}{\tau_\lambda^{\text{anh}}} + \frac{1}{\tau_\lambda^{\text{iso}}}, \tag{4}$$

where $\tau_\lambda^{\text{anh}}$ and $\tau_\lambda^{\text{iso}}$ are anharmonic three-phonon scattering and isotopic scattering, respectively.[5] It can be seen from Fig. 5(b) that the relaxation times of the acoustic mode are much larger than that of the optical mode, which means that the lattice thermal conductivity κ_L is mainly contributed by the acoustic mode, in addition, the acoustic mode relaxation times of K_3IO are quite short, even shorter than previous classic thermoelectric materials such as PbTe.[30] From Eqs. (1) and (2), we can find that the relaxation time τ_λ is directly proportional to the lattice thermal conductivity κ_L. This can further explain why K_3IO has a smaller lattice thermal conductivity κ_L than PbTe.

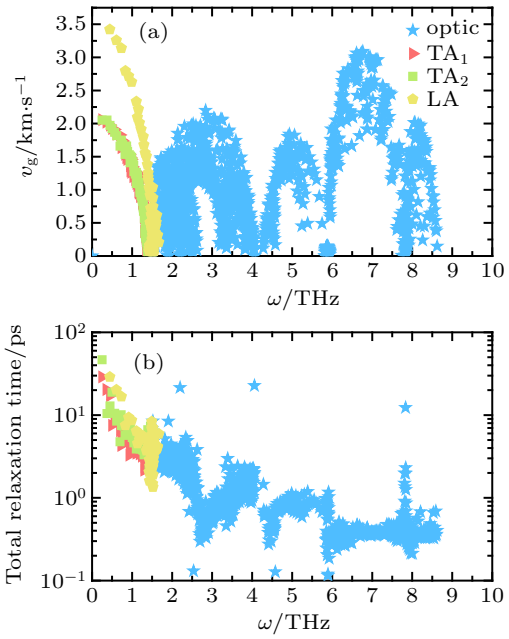


Fig. 5. Phonon group velocities (a) and total relaxation time (b) of all phonon modes as a function of frequency for K_3IO at 300 K, the blue five-pointed stars, red triangles, yellow squares and green pentagons represent optic, TA_1, TA_2 and LA modes, respectively.

As shown in Table 1, we compare the lattice thermal conductivity κ_L, cutoff frequency, sound velocity υ_s and maximal phonon lifetime τ of K_3IO at 300 K with PbTe and Na_2MgSn, where the sound velocity is the average phonon group velocity. We can find that K_3IO has very low κ_L, which, we believe, is due to its relatively low υ_s. The extremely low lattice thermal conductivity usually means higher figure of merit zT and TE conversion efficiency.

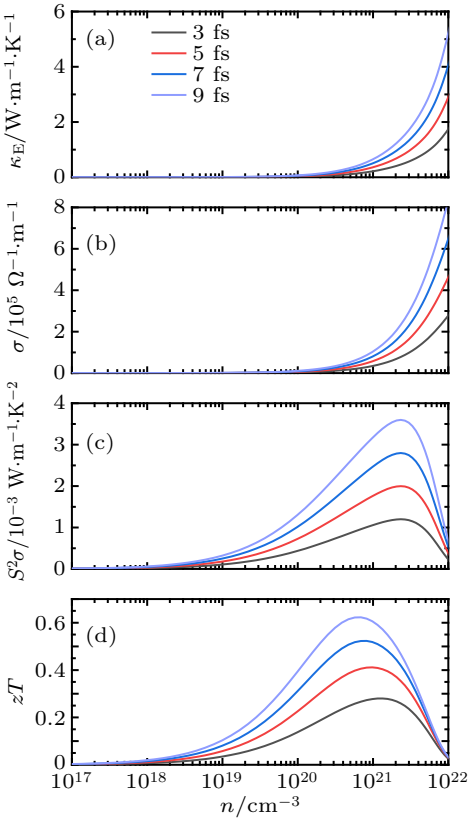


Fig. 6. (a) Electronic thermal conductivity κ_E, (b) electrical conductivity σ, (c) power factor $S^2\sigma$ and (d) figure of merit, zT, of p-type doped K_3IO at 300 K. The black, red, blue and purple curves represent the electronic scattering times of 3 fs, 5 fs, 7 fs and 9 fs, respectively.

In order to better study the electronic transport and TE properties of K_3IO, we use the BOLTZTRAP code to calculate the Seebeck coefficient S and the electrical conductivity σ as functions of temperature T and carriers' concentration n for K_3IO. Considering the influence of electron scattering time τ, we use a simple formula $\tau \sim d/\upsilon$ to estimate the amplitude of electron scattering time τ, where d is the average electron-electron distance estimated by the doping concentration n, and υ is given by $\upsilon = \frac{1}{\hbar}\frac{\partial E}{\partial k}$. For p-type doped K_3IO, the doping concentration $n \sim 10^{21}$ cm^{-3} and the electron velocity $\upsilon \sim 10^5$ m/s, the obtained τ is about 10 fs. Taking into account the influence of scattering mechanisms such as impurity scattering and lattice vibration, the actual electron scattering time τ will be shortened.[5,20,34] In this study, we use τ of 3 fs, 5 fs, 7 fs and 9 fs for calculation and the result is shown in Fig. 6, electronic thermal conductivity κ_E, electrical conductivity σ, power factor $S^2\sigma$ and figure of merit zT increase with the increase of electron scattering time τ. The maximum value of zT is 0.28 (1.34×10^{21} cm^{-3}), 0.41 (9.77×10^{20} cm^{-3}), 0.52 (8.24×10^{20} cm^{-3}) and 0.62 (6.90×10^{20} cm^{-3}) with τ of 3 fs, 5 fs, 7 fs and 9 fs, respectively.

Table 1. Comparison of lattice thermal conductivity κ_L, cutoff frequency, sound velocity υ_s and maximal phonon lifetime τ of K_3IO at 300 K with other TE materials. Here a, b ($a = b$ for the hexagonal structure) and c in parentheses indicate lattice constants.

Material	κ_L/(W/mK)	Cutoff frequency/THz	υ_s/(km/s)	τ/ps
K_3IO	0.93	8.64	0.95	46.5
Na_2MgSn[33]	1.77(a)/0.81(c)	7.27	2.75(a)/2.41(c)	4.5
PbTe[27]	2.1	4.48	1.98[45]	100

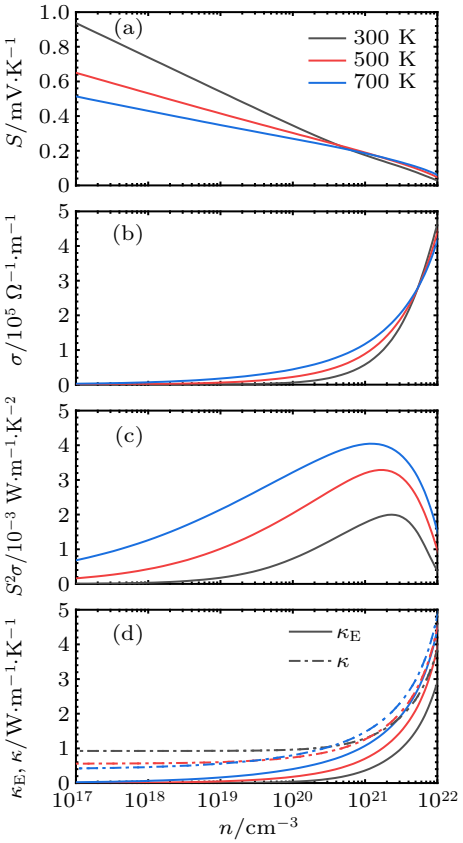


Fig. 7. Thermoelectric parameters of p-type doped K_3IO as a function of carrier concentration with a electronic scattering time of 5 fs. (a) Seebeck coefficient S. (b) Electrical conductivity σ. (c) Power factor $S^2\sigma$. (d) Electronic thermal conductivity κ_E (solid line) and total thermal conductivity κ (dashed line). The temperatures of 300 K, 500 K and 700 K are represented by black, red and blue curves, respectively.

The TE properties of K_3IO at high temperatures are calculated with the electron scattering time takes a fixed value of 5 fs and we use the *ab initio* MD to confirm the kinetic stability of K_3IO at high temperature[44] (see Fig. S2 in the Supplementary Material). The results show that the p-type K_3IO exhibits excellent TE properties, while the results of n-type K_3IO are relatively poor, so no further research is performed here. The calculated S and σ of p-type doped K_3IO as a function of temperature T and carriers' concentration n are plotted in Figs. 7(a) and 7(b), respectively. From Fig. 7(a), the value of Seebeck coefficient S decreases with T at the same n before 3.85 cm^{-3}, as the temperature increases, the decrease in the Seebeck coefficient indicates that there is compensation between the hole and the electron,[31] and it has little change with T after 3.85 cm^{-3}, the value of S decreases with n at the same T. The conductivity σ changes little with T, and increases with n. The power factor $S^2\sigma$ is an important parameter, which gives the information of the effectiveness of thermoelectric materials, the power factor $S^2\sigma$ as a function of carrier concentration n is displayed in Fig. 7(c). We find that the maximum values of $S^2\sigma$ are 2.00×10^{-3} W·m^{-1}·K^{-2} ($n = 2.34\times10^{21}$ cm^{-3}), 3.29×10^{-3} W·m^{-1}·K^{-2} ($n = 1.80\times10^{21}$ cm^{-3}) and 4.04×10^{-3} W·m^{-1}·K^{-2} ($n = 1.15\times10^{21}$ cm^{-3}) at 300 K, 500 K and 700 K, respectively. This high-value power factor predicts the effective heat generation or extraction of K_3IO at an appropriate carrier concentration. The electronic thermal conductivity κ_E and total thermal conductivity κ are shown in Fig. 7(d), from $\kappa = \kappa_E + \kappa_L$, we can find that the lattice thermal conductivity κ_L decreases with the increase of carrier concentration n.

The dimensionless figure of merit, zT, plays a crucial role in predicting the efficiency of thermoelectric application materials,[29] which is mathematically calculated from $zT = S^2\sigma T/\kappa$. By combining the TE parameters in Fig. 7, we plot the value of dimensionless figure of merit, zT, with carrier concentration n in Fig. . The maximum values of zT are 0.41, 1.47 and 2.87 for the corresponding carrier concentrations of 9.77×10^{20} cm^{-3}, 2.51×10^{20} cm^{-3} and 4.68×10^{19} cm^{-3} at the temperature of 300 K, 500 K and 700 K, respectively. We get a relatively large $zT_{700\ K} = 2.87$, which is larger than classic TE material PbTe ($zT = 2.5$).[32] K_3IO also has good TE properties at room temperature, the value of $zT_{300\ K} = 0.41$ is larger than the potential room temperature TE materials Na_2MgSn ($zT_{300\ K} = 0.36$)[33] and $BiCuTe_{0.9}Se_{0.1}O$ ($zT_{300\ K} = 0.3$).[41] Through the calculation of dimensionless figure of merit, zT, we can realize that K_3IO is an excellent TE material and it is a promising candidate for applications in fields in terms of thermoelectricity.

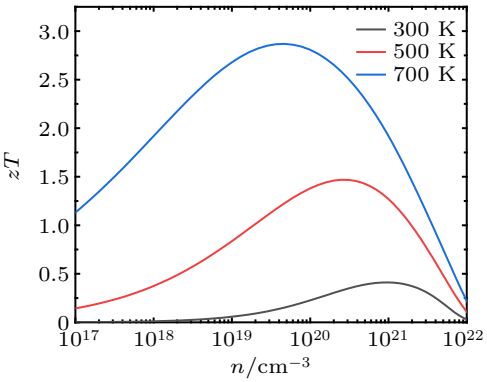


Fig. 8. Figure of merit, zT, as a function of carrier concentration. The temperatures of 300 K, 500 K and 700 K are represented by black, red and blue curves, respectively.

4. Conclusion

In summary, we have investigated and calculated the thermoelectric properties of K_3IO based on first-principles calculations and Boltzmann transport equations. The direct band gap semiconductor K_3IO belongs to the cubic crystal system with the space group of $Pm\bar{3}m$ [221]. The lattice constant,

band gap and Debye temperature are 5.38 Å, 1.02 eV and 80.29 K, respectively. The RTA result of lattice thermal conductivity κ_L is 0.93 $W{\cdot}m^{-1}{\cdot}K^{-1}$ at 300 K, which is lower than the value 1.26 $W{\cdot}m^{-1}{\cdot}K^{-1}$ of the classical TE material PbTe. This is due to the smaller phonon group velocity v_g and smaller relaxation time τ_λ. We use the BOLTZTRAP code to calculate the electronic transport properties based on the semi-classical Boltzmann theory and the rigid-band approach. The electron scattering time takes a fixed value of 5 fs. By calculating and combining the electrical conductivity σ, Seebeck coefficient S, and thermal conductivity κ, we obtain the excellent figure of merit, $zT = 2.87$, of K_3IO at 700 K, which is larger than the classic TE material PbTe ($zT = 2.5$), and the $zT = 0.41$ at 300 K indicates that K_3IO is a potentially excellent room-temperature TE material. Our research on K_3IO shows that it has excellent thermoelectric properties and is a promising candidate for applications in fields in terms of thermoelectricity.

References

[1] Dresselhaus M S, Chen G, Tang M Y, Yang RG, Lee H, Wang DZ, Ren ZF, Fleurial J P and Gogna P 2007 *Adv. Mater.* **19** 1043
[2] Heremans J P, Jovovic V, Toberer E S, Saramat A, Kurosaki K, Charoenphakdee A, Yamanaka S and Snyder G J 2008 *Science* **321** 554
[3] Zebarjadi M, Esfarjani K, Dresselhaus M S, Ren Z F and Chen G 2012 *Energy Environ. Sci.* **5** 5147
[4] Snyder G J and Toberer E S 2008 *Nat. Mater.* **7** 105
[5] Zhao Y C, Dai Z H, Zhang C, Lian C, Zeng S M, Li G, Meng S and Ni J 2017 *Phys. Rev. B* **95** 014307
[6] Mao J, Liu Z H and Ren Z F 2016 *Nature* **1** 1
[7] Hicks L and Dresselhaus M 1993 *Phys. Rev. B* **47** 16631
[8] Harman T C, Walsh M P, Laforge B E and Turner G W 2005 *J. Electron. Mater.* **34** L19
[9] Venkatasubramanian R, Siivola E, Colpitts T and O'quinn B 2001 *Nature* **413** 597
[10] Aronov D, Andalman A S and Fee M S 2008 *Science* **320** 630
[11] Zhao L D, Lo S H, Zhang Y S, Sun H, Tan G J, Uher C, Wolverton C, Dravid V P and Kanatzidis M G 2014 *Nature* **508** 373
[12] Wang H, Bahk J H, Kang C, Hwang J, Kim K, Kim J, Burke P, Bowers J E, Gossard A C, Shakouri A 2014 *Proc. Natl. Acad. Sci. USA* **111** 10949
[13] Kresse G and Furthmüller J 1996 *Phys. Rev. B* **54** 11169
[14] Li W, Carrete J, Katcho N A and Mingo N 2014 *Comput. Phys. Commun.* **185** 1747
[15] Togo A, Oba F and Tanaka I 2008 *Phys. Rev. B* **78** 134106
[16] Kresse G and Joubert D 1999 *Phys. Rev. B* **56** 1758
[17] Chen X, Parker D, Du M H and Singh D J 2013 *New J. Phys.* **15** 043029
[18] Perdew J P, Burke K and Ernzerhof M 1996 *Phys. Rev. Lett.* **77** 3865
[19] He J, Amsler M, Xia Y, Naghavi S S, Hegde V I, Hao S Q, Goedecker S, Ozoliņš V and Wolverton C 2016 *Phys. Rev. Lett.* **117** 046602
[20] Tan X J, Liu W, Liu H J, Shi J, Tang X F and Uher C 2012 *Phys. Rev. B* **85** 205212
[21] Madsen G K and Singh D J 2006 *Comput. Phys. Commun.* **175** 67
[22] Parker D and Singh D J 2012 *Phys. Rev. B* **85** 125209
[23] Togo A and Tanaka I 2015 *Scr. Mater.* **108** 1
[24] Kandemir A and Sahin H 2018 *Phys. Rev. B* **97** 155410
[25] Zhong Q, Dai Z H, Liu J Y, Zhao Y C and Meng S 2020 *Physica E* **115** 113683
[26] Zeeshan M, Singh H K, Van D B J and Kandpal H C 2017 *Phys. Rev. Mater.* **1** 075407
[27] Tian Z T, Garg J, Esfarjani K, Shiga T, Shiomi J and Chen G 2012 *Phys. Rev. B* **85** 184303
[28] Liu J Y, Dai Z H, Yang X X, Zhao Y C and Meng S 2018 *J. Nucl. Mater.* **551** 11
[29] Pei Y Z, Shi X Y, LaLonde A, Wang H, Chen L D and Snyder G J 2011 *Nature* **473** 66
[30] Tian Z T, Garg J, Esfarjani K, Shiga T, Shiomi J and Chen G 2012 *Phys. Rev. B* **85** 184303
[31] Kim S W, Kimura Y and Mishima Y 2007 *Intermetallics* **15** 349
[32] Xiao Y and Zhao L D 2018 *npj Quantum Mater.* **3** 1
[33] Wang C, Chen Y B, Yao S H and Zhou J 2019 *Phys. Rev. B* **99** 024310
[34] Yang X X, Dai Z H, Zhao Y C, Liu J Y and Meng S 2018 *J. Phys.: Condens. Matter* **30** 425401
[35] Becke A D and Johnson E R 2006 *J. Chem. Phys.* **124** 221101
[36] Tran F and Blaha P 2009 *Phys. Rev. Lett.* **102** 226401
[37] Lan Y S, Chen X R, Hu C E, Cheng Y and Chen Q F 2019 *J. Mater. Chem. A* **7** 11134
[38] Tao W L, Lan J Q, Hu C E, Cheng Y, Zhu J and Geng H Y 2020 *J. Appl. Phys.* **127** 035101
[39] Shen H, Xu J Y, Ping W J, He Q B, Zhang Y, Jin M and Jiang G J 2012 *Chin. Phys. Lett.* **29** 076501
[40] Liu X K and Tang B 2013 *Chin. Phys. Lett.* **30** 066201
[41] Huang P, You L, Liang X, Zhang J Y and Luo J 2019 *Acta Phys. Sin.* **68** 077201 (in Chinese)
[42] Zhou Y, Zhao Y Q, Zeng Z Y, Chen X R and Geng H Y 2019 *Phys. Chem. Chem. Phys.* **21** 15167
[43] Hong Y, Zhang J C and Zeng X C 2018 *Chin. Phys. B* **27** 036501
[44] Zhao Y C, Chen X, Zulfiqar M and Ni J 2016 *Phys. Lett. A* **380** 475
[45] Joseph E and Amouyal Y 2015 *J. Electron. Mater.* **44** 1460